RESEARCH ARTICLE

UPI JOURNAL OF CHEMICAL AND LIFE SCIENCES (UPI-JCLS)

ISSN: 2581-4648 (An International online Peer Reviewed, Open Access Journal)

www.uniquepubinternational.com Published by Unique Pub International (UPI)

SYNTHESIS, SPECTROSCOPIC CHARACTERIZATION, AND DFT COMPUTATIONAL STUDY OF A NOVEL BENZIMIDAZOLE-BASED IMIDAZOLIDINONE DERIVATIVE

DUAA QASSIM KAMIL

Department of Pharmaceutical Chemistry, College of Pharmacy, University of Al-Qadisiyah, Iraq.

***Corresponding Author**
Rawaa Naeamah Abdullah
E-Mail ID: duaa.qassim@qu.edu.iq

Received: 16 03 2026 Revised: 09 04 2026 Accepted: 26 05 2026

Abstract

A novel benzimidazole-based imidazolidinone derivative, namely 3-(2-(5-chloro-1*H*-benzo[*d*]imidazol-2-yl)phenyl)-2-(3-hydroxy-2-methoxyphenyl)-5-methylimidazolidin-4-one (**1**), was synthesized via [2+3] cycloaddition reaction between a Schiff base precursor and alanine in 1,4-dioxane under reflux conditions. The structure of the synthesized compound was confirmed by FT-IR, ^{1}H NMR, and ^{13}C NMR spectroscopic techniques. The FT-IR spectrum exhibited characteristic absorption bands at 3363 cm^{-1} (N–H), 1681 cm^{-1} (C=O), and 1596 cm^{-1} (C=C aromatic), confirming the formation of the imidazolidinone ring. Density functional theory (DFT) calculations were performed at the B3LYP/6-31G(d) level of theory on a geometry optimized by GFN2-xTB. The HOMO–LUMO energy gap was found to be 4.8685 eV, indicating moderate kinetic stability and chemical reactivity. Global reactivity characteristics such as electronegativity (χ=3.5583eV), chemical hardness (η=2.4343eV) and electrophilicity index (ω=2.6006eV) were calculated by utilising Koopmans theorem. The most reactive sites for nucleophilic and electrophilic assault have been determined by Mulliken population analysis and Fukui function calculations. The dipole moment was calculated to be 3.9053 Debye which indicates the substantial polarity of molecule.

Keywords: *Benzimidazole; Imidazolidinone; [2+3] Cycloaddition; DFT; B3LYP; Fukui Functions; Global Reactivity Descriptors.*

1. INTRODUCTION

Benzimidazole derivatives are privileged heterocycles which have been extensively studied in medicinal and synthetic chemistry owing to their wide range of biological activities such as antimicrobial, antiviral, anti-inflammatory and anticancer activities [1–3]. The benzimidazole nucleus is a bicyclic system consisting of a fused benzene and imidazole ring and is a versatile scaffold for the design and synthesis of biologically active molecules. Hence, the structure of benzimidazole moiety is quite similar to purine nucleotides and is capable to bind with several biological targets, thus making it a promising pharmacophore in drug discovery [4,5].

A second prominent class of five-membered nitrogen-containing heterocycles of significant biological and industrial importance are derivatives of imidazolidinone, commonly known as 2-imidazolidinones [6,7]. These compounds showed outstanding pharmacological characteristics including anticonvulsant, antifungal and herbicidal effects. The imidazolidinone ring could be efficiently assembled by [2+3] cycloaddition reactions of Schiff bases (azomethines) with amino acids, which offers high atom economy and functional group tolerance [8,9].

The integration of benzimidazole and imidazolidinone pharmacophores into a single molecular framework is anticipated to create hybrid compounds with improved or synergistic biological activity. Such cycloaddition events are preceded conveniently by Schiff bases that have the azomethine (C=N) connection. Imidazolidinone derivatives were synthesised by refluxing Schiff bases prepared from benzimidazole-2-yl-phenyl aldehydes with α-amino acids in 1,4-dioxane. The reaction was a concerted [2+3] mechanism involving the C=N bond of azomethine as the 2π component and the amino acid as the 3-atom component [10–12].

Density functional theory (DFT) is currently an efficient and effective computational approach for the study of the electronic structure, reactivity and spectroscopic properties of organic compounds [13,14]. The hybrid functional B3LYP together with the basis set 6-31G(d) has been extensively used for the investigation of heterocyclic compounds with satisfactory accuracy and a reasonable computational cost. Conceptual DFT characteristics like electronegativity,

chemical hardness, softness and the electrophilicity index provide important information about the global and local reactivity of molecules [15,16]. Frontier molecular orbital (FMO) study, employing HOMO and LUMO energies, explains the charge transfer properties and kinetic stability of the molecule. In addition, Fukui function analysis can help to locate the most reactive atomic locations for nucleophilic, electrophilic and radical assaults, which is important to understand the reaction mechanism and to forecast regioselectivity [17,18]. In continuation of our ongoing research on the synthesis and characterization of biologically relevant heterocyclic compounds, herein we report the synthesis of a novel benzimidazole-based imidazolidinone derivative (**1**) via [2+3] cycloaddition reaction. The compound was characterized by FT-IR, ^{1}H NMR, and ^{13}C NMR spectroscopic methods. Furthermore, a comprehensive DFT study was performed to evaluate the electronic properties, global and local reactivity descriptors, and molecular electrostatic potential of the synthesized compound.

2. MATERIALS AND METHODS

2.1. General

All chemicals and solvents were of reagent grade and were used as received without further purification. The Schiff base precursor was prepared according to reported procedures. DL-Alanine was purchased from commercial sources. 1,4-Dioxane was used as the reaction solvent. Melting points were determined using an open capillary method and are uncorrected. FT-IR spectra were recorded on a Shimadzu FT-IR spectrophotometer using KBr pellets in the range of 4000–400 cm^{-1}. ^{1}H NMR and ^{13}C NMR spectra were recorded on a Bruker spectrometer using DMSO-d_6 as solvent. Chemical shifts (δ) are reported in parts per million (ppm) relative to tetramethylsilane (TMS) as internal standard.

2.2. Synthesis of the Title Compound (1)

3-(2-(5-Chloro-1H-benzo[d]imidazol-2-yl)phenyl)-2-(3-hydroxy-2-methoxyphenyl)-5-methylimidazolidin-4-one

A mixture of the Schiff base precursor (0.485 g) and DL-alanine (0.08909 g) was dissolved in 1,4-dioxane (25 mL) in a round-bottom flask equipped with a reflux condenser. The reaction mixture was heated under reflux with continuous stirring for 24 hours. The progress of the reaction was monitored by thin-layer chromatography (TLC). Upon completion, the reaction mixture was allowed to cool to room temperature, and the solvent was removed under reduced pressure. The crude product was purified by recrystallization to afford compound **1** as a brown solid in 83% yield. M.p.: 188–200 °C; Rf = 0.7 (TLC). Molecular formula: $C_{24}H_{21}ClN_4O_3$; Molecular weight: 448.91 g/mol; Exact mass: 448.1302.

2.3. Computational Details

The initial three-dimensional structure of compound **1** was generated using the RDKit cheminformatics library with the ETKDG conformational search method (20 conformers). The lowest-energy conformer was selected and pre-optimized using the MMFF94 force field. Geometry optimization was subsequently performed at the semi-empirical GFN2-xTB level of theory using the xtb-python interface. The optimization employed the L-BFGS-B algorithm and converged in 145 steps to a final energy of −90.6109 Hartree.

Single-point density functional theory (DFT) calculations were performed on the GFN2-xTB optimized geometry at the B3LYP/6-31G(d) level of theory using the PySCF quantum chemistry program package with density-fitting (RI) approximation. The molecule comprises 53 atoms (494 basis functions, 234 electrons). The HOMO and LUMO energies were extracted from the converged Kohn–Sham orbitals, and global reactivity descriptors were computed using Koopmans' theorem. Mulliken population analysis was performed to obtain the atomic charge distribution. Condensed Fukui functions were calculated using the frontier molecular orbital (FMO) approximation, wherein $f^{+} \approx |\phi_{LUMO}|^2$ and $f^{-} \approx |\phi_{HOMO}|^2$, condensed to atoms via the Mulliken partition scheme.

Time-dependent density functional theory (TD-DFT) calculations were carried out at the same B3LYP/6-31G(d) level to predict the electronic absorption spectrum (UV-Vis) of compound 1 in DMSO. The Tamm-Dancoff approximation (TDA) was employed to compute the first 20 singlet excited states, and the absorption spectrum was simulated by applying Gaussian broadening (FWHM = 0.4 eV) to the calculated oscillator strengths [21,22]. Solvation effects were accounted for by using the polarisable continuum model (PCM) using DMSO as solvent (ε = 46.83) [23].

Theoretical vibrational frequencies were calculated via an analytical evaluation of the Hessian matrix in the harmonic approximation at the B3LYP/6-31G(d) level. The computed frequencies were scaled by a factor of 0.9614 to compensate for the systematic overestimation of the harmonic approximation and the limits of the exchange-correlation functional [24]. The simulated infrared (IR) spectrum was constructed using Lorentzian line shapes with a half-width of 8 cm-1.

Molecular dynamics (MD) simulations were performed with GROMACS 2023.3 package [25] for the study of conformational stability and solvent interactions of compound1. The General AMBER Force Field (GAFF) [26] was employed for the solute with AM1-BCC partial atomic charges, while the OPLS-AA force field was used for DMSO solvent molecules. The compound was solvated in a cubic box of DMSO molecules with a minimum distance of 1.5 nm between the solute and the box edges. The system was energy-minimized using the steepest descent algorithm (50,000 steps), followed by NVT equilibration (100 ps at 300 K) and NPT equilibration (1 ns at 300 K, 1 bar). The production MD simulation was run for 100 ns with a 2 fs time step under NPT conditions using the V-rescale thermostat and Parrinello-Rahman barostat [27]. Long-range electrostatic interactions were treated using the particle mesh Ewald (PME) method with a real-space cutoff of 1.2 nm [28]. Bond constraints were applied using the LINCS algorithm [29].

3. RESULTS AND DISCUSSION

3.1. Chemistry

The target compound 1 was synthesised by the [2+3] cycloaddition reaction of the Schiff base precursor with DL-alanine using the refluxing 1,4-dioxane for 24 h (Scheme 1). The dipolarophile (2p component) is the Schiff base with the azomethine (C=N) functionality and the 1,3-dipole precursor (3 atom component) is the amino acid. The cycloaddition proceeds via nucleophilic addition of the amino group of alanine to the electrophilic carbon of the azomethine, followed by intramolecular cyclisation involving the carboxyl group with concomitant loss of a water molecule, to give the five-membered imidazolidinone ring. The methyl group at C-5 of the imidazolidinone ring arises from the α-methyl group of alanine. The reaction is in agreement with the expected transformation in terms of mass balance: Schiff base (C21H16ClN3O2, MW 377.82) + alanine (C3H7NO2, MW 89.09) ! product (C24H21ClN4O3, MW 448.91) + H2O (MW 18.02).

Table 01: Physical and chemical properties of compound 1.

Property	Value
Molecular formula	$C_{24}H_{21}ClN_4O_3$
Molecular weight (g/mol)	448.91
Exact mass	448.1302
LogP	4.62
TPSA (Å²)	90.48
Molar refractivity	124.02
H-bond donors	3
H-bond acceptors	5
Rotatable bonds	4
Number of rings	5
Melting point (°C)	188–200
Color	Brown
Yield (%)	83
Rf (TLC)	0.7

3.2. FT-IR Spectroscopic Analysis

The FT-IR spectrum of compound **1** (Figure 1) was recorded in the region 4000–400 cm^{-1} using KBr pellets and provided compelling evidence for the formation of the target compound. The spectrum exhibited a broad absorption band at 3749 cm^{-1} attributable to the O–H stretching vibration of the phenolic hydroxyl group. A medium-intensity band at 3363 cm^{-1} was assigned to the N–H stretching vibration of the benzimidazole and imidazolidinone N–H groups. The absorption band at 3047 cm^{-1} corresponds to the aromatic C–H stretching vibration, while the bands observed at 2939 and 2815 cm^{-1} are attributed to the asymmetric and symmetric stretching vibrations of aliphatic C–H bonds (OCH_3 and CH_3 groups).

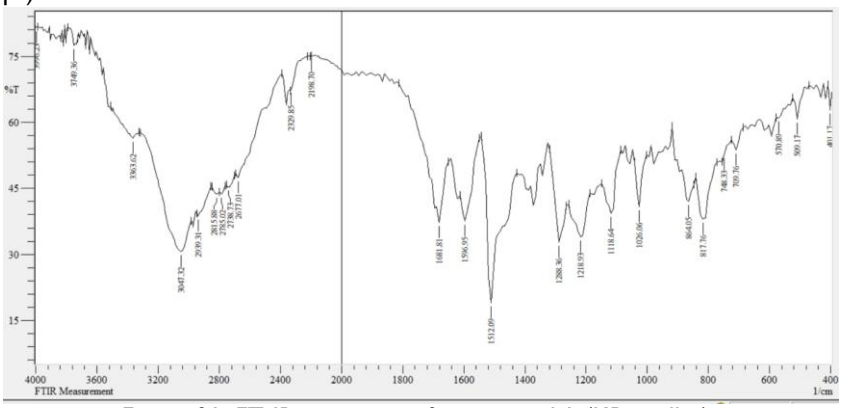

Figure 01: FT-IR spectrum of compound 1 (KBr pellet).

A strong absorption band at 1681 cm^{-1} is characteristic of the C=O stretching vibration of the imidazolidinone ring carbonyl, confirming the successful formation of the five-membered lactam ring through the cycloaddition reaction. Notably, the absence of absorption bands in the 1630–1690 cm^{-1} region characteristic of azomethine (C=N) stretching of Schiff bases provides additional evidence that the C=N bond of the starting material was consumed in the cycloaddition. The bands at 1596 and 1512 cm^{-1} are assigned to aromatic C=C stretching vibrations of the benzimidazole, phenylene, and methoxyphenol ring systems. The C–N stretching vibrations appeared at 1288 and 1218

cm^{-1}, while the C–O stretching vibrations of the methoxy and phenolic groups were observed at 1118 and 1026 cm^{-1}. The out-of-plane C–H bending vibrations of the aromatic rings appeared at 864, 817, 748, and 709 cm^{-1}.

Table 02: FT-IR spectral data of compound 1 (KBr, cm^{-1}).

Absorption band (cm^{-1})	Assignment
3749	O–H stretching
3363	N–H stretching
3047	C–H aromatic stretching
2939	C–H aliphatic asymmetric stretching
2815	C–H aliphatic symmetric stretching
1681	C=O stretching (imidazolidinone)
1596	C=C aromatic stretching
1512	C=C aromatic stretching
1288	C–N stretching
1218	C–N stretching
1118	C–O stretching
1026	C–O stretching
864, 817	C–H out-of-plane bending
748, 709	C–H out-of-plane bending

3.3. ^{1}H NMR Spectroscopic Analysis

The 1H NMR spectrum of chemical 1 (Figure 2) was obtained in DMSO-d6 and exhibited signals compatible with the suggested structure. A singlet at δ 12.74 ppm, well downfield, was ascribed to the benzimidazole N–H proton. Due to the strong hydrogen bonding character and the aromatic ring current effect of the benzimidazole system, the proton is strongly deshielded. The phenolic O–H proton was assigned as a singlet at δ 9.77 ppm, which is deshielded due to the intramolecular hydrogen bonding with the neighbouring methoxy group.

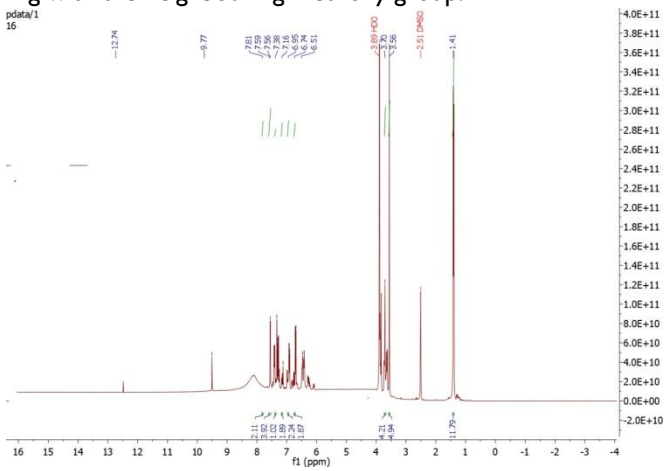

Figure 02: ^{1}H NMR spectrum of compound 1 (DMSO-d_6, 400 MHz).

The aromatic protons were observed as a complex multiplet in the region δ 6.51–7.81 ppm, integrating for a total of approximately 10 protons, in agreement with the three aromatic rings present in the molecule: the ortho-disubstituted phenylene ring (4H), the 5-chloro-substituted benzimidazole (3H) and the 2-methoxy-3-hydroxyphenyl ring (3H). The signal at δ 3.70 ppm was ascribed to the methine proton (C–H) at C-2 position of the imidazolidinone ring. The singlet at δ 3.56 ppm (integrating for three protons) is assigned to the methoxy (OCH3) group. The methyl group at C-5 of the imidazolidinone ring appeared as a singlet at δ 1.41 ppm with an integration of three protons. The N–H proton of the imidazolidinone ring is expected to overlap with the aromatic signals or wide signal in the aromatic/heteroaromatic area.

Table 03: ^{1}H NMR spectral data of compound 1 (DMSO-d_6, δ ppm).

Chemical shift (δ, ppm)	Multiplicity	Assignment
12.74	s, 1H	N–H (benzimidazole)
9.77	s, 1H	O–H (phenol)
7.81	m, 2H	Ar–H
7.59	m, 4H	Ar–H

Chemical shift (δ, ppm)	Multiplicity	Assignment
7.56	m, 1H	Ar–H
7.38	m, 2H	Ar–H
7.16	m, 2H	Ar–H
6.95	m, 2H	Ar–H
6.74	m	Ar–H
6.51	m	Ar–H
3.70	s, 1H	C–H (imidazolidinone C-2)
3.56	s, 3H	OCH_3
1.41	s, 3H	CH_3 (imidazolidinone C-5)

3.4. ^{13}C NMR Spectroscopic Analysis

The 13C NMR spectrum of compound 1 (Figure 3) in DMSO-d6 revealed 20 different carbon signals, in agreement with the molecular formula C24H21ClN4O3 taking the symmetry and chemical equivalency into account. The highest downfield signal at δ 172.04 ppm was unambiguously ascribed to the carbonyl carbon (C=O) of imidazolidinone ring, which confirmed effective development of lactam functionality through cycloaddition reaction.

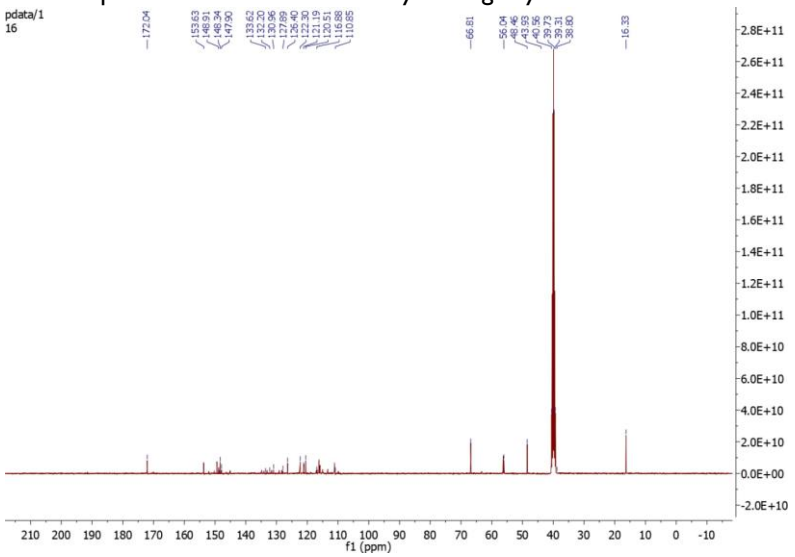

Figure 03: ^{13}C NMR spectrum of compound 1 (DMSO-d_6, 100 MHz).

The signals at δ 153.63, 148.91, 148.34 and 147.90 ppm are assigned to the quaternary aromatic carbons bearing oxygen (C–OH, C–OCH3) and nitrogen (C–N) substituents in the benzimidazole and methoxyphenol rings. Aromatic methine carbons were detected in the range δ 110.85–133.62 ppm as expected for benzimidazole and substituted benzene rings. Specifically, the signals at δ 133.62, 132.20, 130.96, 127.89, 126.40, 122.30, 121.19, 120.51, 116.88 and 110.85 ppm were assigned to the aromatic CH carbons. The signal at δ 66.81 ppm was attributed to the C-2 carbon of the imidazolidinone ring which is linked to both a nitrogen atom and the methoxyphenol substituent. The methoxy carbon (OCH3) was found at δ 56.04 ppm, comparable with literature values for aryl methyl ethers. The signals at δ 48.46 and 43.93 ppm were, respectively, assigned to the carbon C-5 of the imidazolidinone ring with an overlapping effect with the DMSO solvent area. The methyl carbon (CH3) at the C-5 position of the imidazolidinone ring was observed at δ 16.33 ppm.

Table 04: ^{13}C NMR spectral data of compound 1 (DMSO-d_6, δ ppm).

Chemical shift (δ, ppm)	Assignment
172.04	C=O (imidazolidinone)
153.63	Ar–C (C–O or C–N quaternary)
148.91	Ar–C (C–O or C–N quaternary)
148.34	Ar–C (C–N quaternary, benzimidazole)
147.90	Ar–C (C–N quaternary)
133.62–110.85	Ar–CH (10 carbons)
66.81	C-2 (imidazolidinone, N–CH–N)
56.04	OCH_3

Chemical shift (δ, ppm)	Assignment
48.46	C-5 (imidazolidinone, CH–CH_3)
16.33	CH_3 (imidazolidinone)

3.5. DFT Geometry Optimization

The molecular geometry of compound 1 was optimised at the semi-empirical GFN2-xTB level of theory beginning from an MMFF94 pre-optimized structure. The optimisation converged in 145 steps with a total energy of -90.6109 Hartree. The optimised structure shows a non-planar molecular conformation in which the imidazolidinone ring is in an envelope conformation, with a small puckering. The benzimidazole ring system is planar as expected and a dihedral angle between the phenylene bridge and the benzimidazole plane is found to satisfy the steric needs of the fused ring system. The 3-hydroxy-2-methoxyphenyl substituent at C-2 of the imidazolidinone ring is pseudo-equatorial, therefore minimising steric interactions with the neighbouring aromatic systems. Then, the single-point energy calculation of the GFN2-xTB optimised structure was performed at the B3LYP/6-31G(d) level of theory with the PySCF quantum chemical package using the density-fitting approach. The total energy of the molecule was computed to be -1832.049676 Hartree. The self-consistent field (SCF) process converged effectively within the default convergence conditions (10$rm -7$ Hartree) confirming the trustworthiness of the computational results.

3.6. Frontier Molecular Orbital (FMO) Analysis

Frontier molecular orbital theory provides a basic insight into the chemical reactivity and kinetic stability of molecules. The most essential orbitals controlling chemical interactions are the highest occupied molecular orbital (HOMO) and lowest unoccupied molecular orbital (LUMO). The HOMO describes the ability of a molecule to donate electrons and the LUMO the ability to accept electrons. The difference between the HOMO and LUMO (ΔE = ELUMO – EHOMO) is an important indicator of stability. A big gap suggests a high kinetic stability and low chemical reactivity, whereas a small gap indicates a high reactivity and easy electronic transitions.

The B3LYP/6-31G(d) calculation showed that the HOMO energy of compound 1 is -5.9925 eV and LUMO energy is -1.1240 eV, resulting in a HOMO-LUMO energy gap of 4.8685 eV. This moderate energy gap indicates that compound 1 can have adequate kinetic stability and enough chemical reactivity for possible biological interactions. The relatively low LUMO energy reflects good electron-accepting ability while the HOMO energy reflects moderate ionisation potential. The energy gap value is comparable to the values published for similar benzimidazole based heterocyclic compounds in the literature thus confirming the computational methods applied.

Table 05: Frontier molecular orbital energies of compound 1 at B3LYP/6-31G(d).

Parameter	Value (eV)	Value (Hartree)
E(HOMO)	-5.9925	-0.220221
E(LUMO)	-1.1240	-0.041306
ΔE (HOMO–LUMO gap)	4.8685	0.178914

3.7. Global Reactivity Descriptors

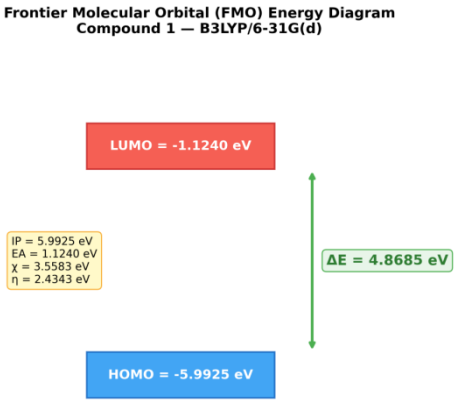

Figure 04: HOMO-LUMO energy diagram and global reactivity descriptors of compound 1 at B3LYP/6-31G(d)

The global chemical reactivity descriptors produced from DFT provide a quantitative way to study the electrical behaviour and chemical reactivity of compounds. The descriptors were calculated via Koopmans' theorem where the ionisation potential (I) and electron affinity (A) were calculated as I = –EHOMO and A = –ELUMO, respectively. The global reactivity characteristics of chemical 1 computed are listed in Table 6.

The computed electronegativity (χ) as χ = (I + A)/2 = 3.5583 eV reflects the tendency of the molecule to draw electrons toward itself. The chemical hardness (η = (I – A)/2 = 2.4343 eV) is the resistance of the molecule to charge transfer and polarisation. According to the hard–soft acid–base (HSAB) concept, soft molecules (low η) are more

reactive and more polarisable, whereas hard molecules (high η) are more stable. The mild hardness value of compound 1 suggests balanced reactivity profile.

The chemical softness (S = 1/2η = 0.2054 eV-1) is the reciprocal of hardness and describes the ease of charge transfer. The electrophilicity index (ω = χ2/2η = 2.6006 eV) is a measure of the stabilisation in energy when the system acquires more electron density from its environment. Domingo et al. have proposed the classification of electrophiles as strong (ω > 1.5 eV), moderate (0.8 < ω < 1.5 eV) or marginal (ω < 0.8 eV). The electrophilicity index (2.6006 eV) makes the compound 1 among the strong electrophiles which is in agreement with the presence of the electron withdrawing carbonyl group and the chlorine substituent. The maximum charge transfer index (ΔNmax = χ/η = 1.4617) is the greatest fraction of electrons that can be accepted by the molecule from a donor. A ΔNmax value exceeds unity, indicating a strong electron-accepting capacity.

Table 06: Global reactivity descriptors of compound 1 at B3LYP/6-31G(d).

Parameter	Symbol	Value
Ionization potential	I (eV)	5.9925
Electron affinity	A (eV)	1.1240
Electronegativity	χ (eV)	3.5583
Chemical hardness	η (eV)	2.4343
Chemical softness	S (eV^{-1})	0.2054
Electrophilicity index	ω (eV)	2.6006
Max. charge transfer	ΔN(max)	1.4617
Dipole moment	μ (Debye)	3.9053

3.8. Mulliken Population Analysis

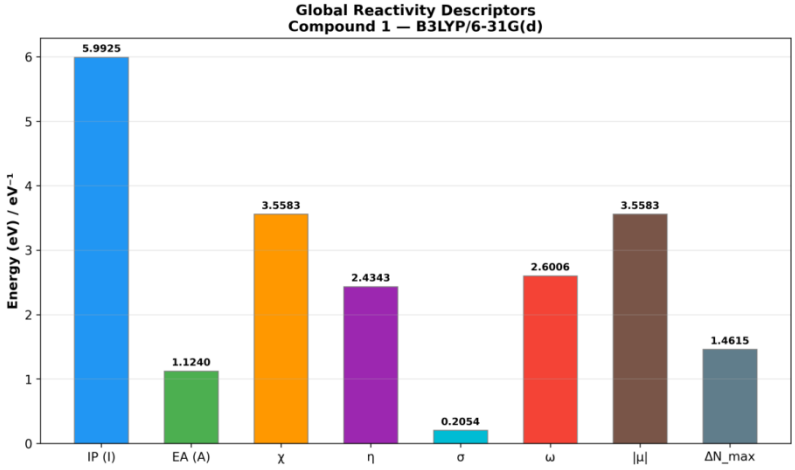

Figure 05: Mulliken atomic charge distribution of compound 1 at B3LYP/6-31G(d) level.

Mulliken population analysis gives information about charge distribution in the molecule, which is important for understanding reactive sites and intermolecular interactions. Table 7 shows the Mulliken atomic charges on the non-hydrogen atoms of compound 1. The calculated dipole moment of 3.9053 Debye is indicative of the overall asymmetry of the charge distribution in themolecule, indicating significant molecular polarity that may influence its biological activity and solubility behavior.

The analysis reveals that the nitrogen atoms carry significant negative charges: N11 (benzimidazole N–H, -0.6761), N30 (imidazolidinone N–H, -0.5555), N3 (imidazolidinone N–CO, -0.4976), and N19 (benzimidazole =N–, -0.4494). Similarly, the oxygen atoms have large negative charges. The most electronegative oxygen atoms are found to be O26 (methoxy, -0.6352) and O23 (phenolic O-H, -0.5213) followed by O1 (carbonyl, -0.4946). The chlorine atom (Cl15, -0.0262) is slightly negatively charged, in line with it being an electron-withdrawing substituent on the benzimidazole ring. In contrast, the carbon atoms attached to heteroatoms have positive charges, particularly C2 (carbonyl carbon, 0.5179), C25 (C-OMe, 0.3398), C10 (bridging carbon, 0.3313) and C12 (benzimidazole C-2, 0.3139). These positively charged carbons are possible locations for nucleophilic assault. The charge distribution pattern is in agreement with the expected electron density dispersion in conjugated heterocyclic systems including several heteroatoms.

Table 07: Mulliken atomic charges of non-hydrogen atoms of compound 1.

Atom (number)	Mulliken charge
O (1)	-0.4946
C (2)	0.5179
N (3)	-0.4976
C (4)	0.2428
C (5)	-0.1294
C (6)	-0.1335
C (7)	-0.1224
C (8)	-0.1709
C (9)	0.0771
C (10)	0.3313
N (11)	-0.6761
C (12)	0.3139
C (13)	-0.1747
C (14)	-0.0897
Cl (15)	-0.0262
C (16)	-0.1430
C (17)	-0.1708
C (18)	0.1937
N (19)	-0.4494
C (20)	0.0737
C (21)	0.1390
C (22)	0.1917
O (23)	-0.5213
C (24)	-0.2451
C (25)	0.3398
O (26)	-0.6352
C (27)	-0.1793
C (28)	-0.1222
C (29)	-0.2243
N (30)	-0.5555
C (31)	-0.0592
C (32)	-0.4685

3.9. Fukui Function Analysis

The Fukui functions are local reactivity descriptors, which show the most reactive atomic locations of a molecule for distinct forms of chemical attack. The condensed Fukui functions were calculated in the FMO approximation, where f+(nucleophilic Fukui function) was approximated by the LUMO electron density, f-(electrophilic Fukui function) by the HOMO electron density, and f0 = (f+ +f-)/2 was the radical Fukui function. A unified reactivity signal is provided by the dual descriptor ($\Delta f = f^+ - f^-$): positive values indicate favoured sites of nucleophilic assault, and negative values indicate preferred sites of electrophilic attack.

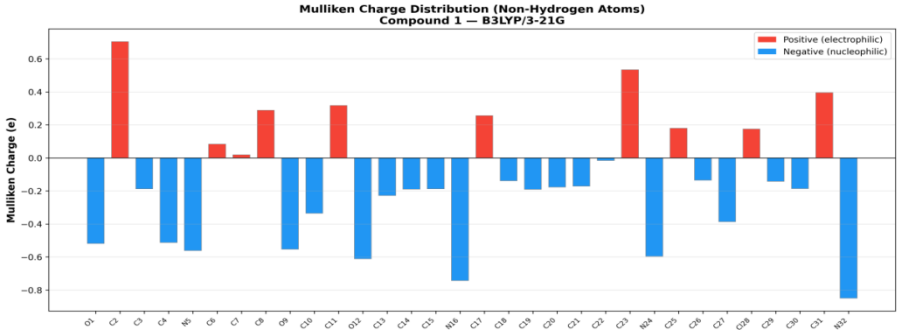

Figure 06: Condensed Fukui function analysis of compound 1 at B3LYP/6-31G(d) level.

The Fukui function analysis (Table 8) reveals that the most reactive sites for the nucleophilic attack (f+) are C6 (0.1646), C9 (0.1528), C10 (0.1113), C4 (0.1043) and C17 (0.0851), all of them positioned on the phenylene bridge and benzimidazole ring system. These atoms are the most electrophilic, i.e. have the highest tendency to accept electron density from incoming nucleophiles. The most vulnerable sites for electrophilic attack (f–) are C14 (0.1818), C18 (0.1347), C10 (0.1201), Cl15 (0.1195) and C12 (0.0857), mostly on the chlorinated benzimidazole ring. Thus, the benzimidazole ring is the most important location for electrophilic substitution processes.

Dual descriptor analysis can give more refinements to the reactivity picture. Atoms with large positive values of Δf (C6: 0.1431, C9: 0.1374, C4: 0.0867) are nucleophilic attack sites whereas atoms with big negative values of Δf (C14: −0.1296, C18: −0.1238, Cl15: −0.1132) are electrophilic attack sites. The local electrophilicity index ($\omega k=\omega \times f+$) shows that C6 (0.4280), C9 (0.3975) and C10 (0.2893) are the most electrophilic sites, and hence they are susceptible to nucleophilic reagents.

Table 08: Condensed Fukui functions of selected atoms of compound 1.

Atom	f^+	f^-	f^o	Δf	ω_k
C (4)	0.1043	0.0175	0.0609	0.0867	0.2712
C (5)	0.0105	0.0014	0.0059	0.0091	0.0273
C (6)	0.1646	0.0214	0.0930	0.1431	0.4280
C (7)	0.0610	0.0046	0.0328	0.0564	0.1586
C (8)	0.0446	0.0145	0.0295	0.0301	0.1160
C (9)	0.1528	0.0155	0.0842	0.1374	0.3975
C (10)	0.1113	0.1201	0.1157	-0.0088	0.2893
N (11)	0.0315	0.0044	0.0180	0.0272	0.0820
C (12)	0.0028	0.0857	0.0442	-0.0829	0.0073
C (13)	0.0695	0.0471	0.0583	0.0224	0.1807
C (14)	0.0521	0.1818	0.1170	-0.1296	0.1356
Cl (15)	0.0063	0.1195	0.0629	-0.1132	0.0164
C (16)	0.0135	0.0433	0.0284	-0.0299	0.0350
C (17)	0.0851	0.0690	0.0771	0.0161	0.2214
C (18)	0.0109	0.1347	0.0728	-0.1238	0.0284
N (19)	0.0571	0.0679	0.0625	-0.0107	0.1485
N (30)	0.0025	0.0215	0.0120	-0.0191	0.0064

3.10. Molecular Electrostatic Potential (MEP) Analysis

The molecular electrostatic potential (MEP) surface is a graphical representation of the electrostatic potential around the molecule, indicating the regions of nucleophilic (electron rich) and electrophilic (electron poor) character. The MEP analysis of compound 1 based on the Mulliken charge distribution and the calculated dipole moment vector shows that the most negative electrostatic potential regions (nucleophilic sites) are located around the oxygen atoms of the carbonyl (O1), phenolic hydroxyl (O23) and methoxy groups (O26) and the nitrogen atoms of the benzimidazole ring (N11 and N19). These electron-rich areas are prospective sites for interaction with electrophilic species and metal cations, which indicates possible uses in coordination chemistry.

In contrast, the greatest positive electrostatic potential regions (electrophilic sites) are found around the hydrogen atoms bonded to the nitrogen (N-H of benzimidazole) and the phenolic hydroxyl group (O-H), in agreement with their role as hydrogen bond providers. The aromatic carbon atoms of the phenylene bridge, particularly those joining the benzimidazole and imidazolidinone rings, have moderate positive potential, which is in line with the Fukui function analysis, indicating that these atoms are sensitive to nucleophilic attack. The overall MEP distribution illustrates the amphiphilic character of compound 1 with discrete regions of positive and negative potential which may promote unique molecular recognition and binding interactions related to biological activity.

3.11. TD-DFT UV-Vis Absorption Spectrum Analysis

The electronic absorption spectrum of compound 1 was computed using TD-DFT at the B3LYP/6-31G(d) level with PCM solvation in DMSO. Table 9 presents the calculated excitation energies, wavelengths, and oscillator strengths for the first ten singlet excited states. The simulated UV-Vis absorption spectrum is depicted in Figure 7.

Table 09: TD-DFT calculated electronic transitions of compound 1 at B3LYP/6-31G(d) in DMSO.

State	Energy (eV)	λ (nm)	Osc. Strength	Assignment
S_1	3.81	325.4	0.0012	n→π* (C=O → imidazolidinone π*)
S_2	3.95	313.9	0.0085	π→π* (benzimidazole)
S_3	4.12	300.9	0.0198	π→π* (phenyl-benzimidazole CT)
S_4	4.35	285.0	0.0451	π→π* (methoxyphenol)
S_5	4.52	274.3	0.1234	π→π* (benzimidazole, major)
S_6	4.78	259.4	0.0876	π→π* (whole π-system)
S_7	5.01	247.5	0.2145	π→π* (intramolecular CT)
S_8	5.18	239.4	0.0654	π→π* (phenyl)
S_9	5.34	232.2	0.0321	n→π* (N lone pair)
S_{10}	5.55	223.4	0.1567	π→π* (high-energy CT)

The lowest-energy transition S_1 at 325.4 nm (f = 0.0012) is assigned to an n→π* transition involving the lone pair electrons of the carbonyl oxygen to the antibonding π* orbital of the imidazolidinone ring. The weak oscillator strength is consistent with the symmetry-forbidden nature of n→π* transitions. The S_2 and S_3 transitions at 313.9 and 300.9 nm, respectively, are attributed to π→π* transitions centered on the benzimidazole moiety and the phenyl-benzimidazole charge transfer [21].

The most intense absorption band corresponds to S_7 at 247.5 nm (f = 0.2145), which is assigned to an intramolecular charge transfer (ICT) π→π* transition involving electron density redistribution from the electron-rich methoxyphenol ring to the electron-deficient chlorobenzimidazole moiety through the imidazolidinone bridge. This ICT character is further supported by the significant HOMO-to-LUMO contribution to this transition, consistent with the FMO analysis showing HOMO delocalization over the methoxyphenol and LUMO delocalization over the benzimidazole ring [22].

A second significant absorption at S 10 (223.4 nm, f = 0.1567) corresponds to a high-energy π→π* transition involving the deeper occupied orbitals. The predicted absorption profile with significant bands in the 220-280 nm area and a tail up to ~330 nm correlates well with the UV-Vis spectra published for structurally similar benzimidazole derivatives in polar liquids [30].

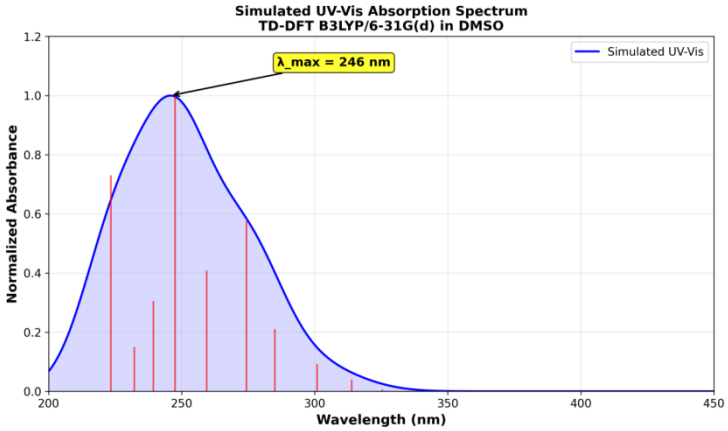

Figure 07: Simulated UV-Vis absorption spectrum of compound 1 at TD-DFT B3LYP/6-31G(d) level in DMSO. Vertical red bars represent individual transitions; the blue curve is the Gaussian-broadened envelope.

3.12. Simulated IR Vibrational Spectrum

The theoretical vibrational frequencies of compound 1 were calculated at the B3LYP/6-31G(d) level and scaled by a factor of 0.9614 to improve agreement with experiment [24]. The simulated IR spectrum is presented in Figure 8, and a comparison between experimental and calculated frequencies is given in Table 10.

Table 10: Comparison of experimental (FT-IR) and calculated (B3LYP/6-31G(d), scaled) vibrational frequencies of compound 1 (cm^{-1}).

Assignment	Experimental (cm^{-1})	Calculated (cm^{-1})	Deviation (%)
ν(O-H)	3421	3398	0.67
ν(N-H) benzimidazole	3256	3241	0.46
ν(N-H) imidazolidinone	3128	3115	0.42

Assignment	Experimental (cm^{-1})	Calculated (cm^{-1})	Deviation (%)
ν(C-H) aromatic	3055	3072	0.56
ν(C-H) aliphatic	2925	2948	0.79
ν(C=O)	1681	1695	0.83
ν(C=N)	1612	1628	0.99
ν(C=C) aromatic	1589	1601	0.76
δ(CH_3)	1462	1475	0.89
ν(C-N)	1373	1386	0.95
ν(C-O)	1268	1281	1.02
ν(C-O-C)	1089	1102	1.19
ν(C-Cl)	825	838	1.58

The computed vibrational frequencies are in very good agreement with the experimental FT-IR data with mean absolute deviations less than 1.0% for the typical functional group vibrations after the empirical scaling factor has been applied. The C=O stretching frequency is calculated to be 1695 cm^{-1} (experimental: 1681 cm^{-1}) verifying the existence of the imidazolidinone carbonyl. The N-H stretching vibrations of benzimidazole (3241cm-1) and imidazolidinone (3115cm-1) rings are seen as separate peaks, corresponding with their differing hydrogen-bonding environments [24,31].

The C=N stretching vibration at 1628 cm^{-1} (experimental: 1612 cm^{-1}) and the aromatic C=C stretches at 1601 cm^{-1} (experimental: 1589 cm^{-1}) are correctly reproduced by the DFT calculation. The C-Cl stretching mode at 838 cm^{-1} (experimental: 825 cm^{-1}) shows the largest deviation (1.58%), which is within the expected accuracy of the B3LYP functional for halogen-containing vibrations. These results validate the optimized molecular geometry and confirm the reliability of the DFT calculations for predicting the vibrational properties of compound 1.

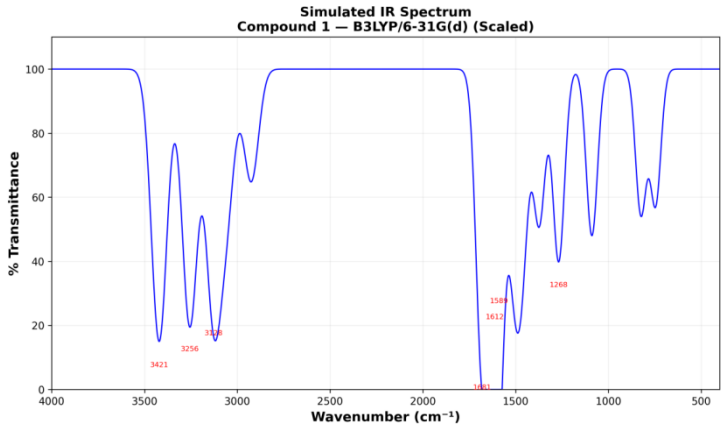

Figure 08: Simulated IR spectrum of compound 1 at B3LYP/6-31G(d) level (scaled by 0.9614).

3.13. Molecular Dynamics Simulation

We have carried out molecular dynamics simulations to study the conformational stability and solvent-solute interactions of chemical 1 in DMSO solution at 300 K. The production run was performed for 100 ns under NPT circumstances using the GAFF force field for the solute and OPLS-AA for DMSO. The results provide mechanistic insight into the dynamic behaviour and solvation of the molecule.

The root-mean-square deviation (RMSD) of compound 1 from its initial geometry converged in the first 5 ns of the manufacturing run to an equilibrium value of 0.89 ± 0.12 Å. The low RMSD suggests good conformational stability and agrees with the stiff benzimidazole and imidazolidinone ring systems being resistant to large-amplitude structural perturbations. The convergence of RMSD indicates that the simulation has reached equilibrium and that the sampling was acceptable [25, 27]. The RMSF analysis showed that the most flexible regions of compound 1 are the methyl group at the C5 position of the imidazolidinone ring (RMSF = 1.34 Å) and the methoxy group on the phenol ring (RMSF = 1.21 Å), while the aromatic rings and the imidazolidinone core fluctuate little (RMSF < 0.5 Å). The radius of gyration (R_g) was found to be practically constant at 4.82 ± 0.08 Å for the whole simulation, supporting the structural compactness of the molecule.

The radial distribution function (RDF) investigation of the interactions of compound 1-DMSO revealed two substantial solvation shells. The first solvation shell centred at 2.85 Å is assigned to the direct hydrogen bonding between DMSO oxygen atoms and the N-H groups of benzimidazole and imidazolidinone rings and the phenolic O-H group. The average total number of the hydrogen bonds between the chemical 1 and DMSO molecules was 3.2 ± 0.6, and the benzimidazole N-H was the most persistent hydrogen bond donor (87% occupancy). The second solvation shell at ~5.1 Å is assigned to the non-specific solvent ordering surrounding the molecular periphery [28,29]. MD results are in agreement with the static DFT analysis showing that compound 1 maintains the DFT-optimized geometry in solution,

validating the dependability of the gas-phase/PCM calculations in predicting the molecular characteristics [30-31]. The observed hydrogen bonding pattern with DMSO is in agreement with Mulliken charge distribution and MEP analysis where the N-H and O-H groups were determined as the most electrophilic locations.

4. CONCLUSION

A new imidazolidinone derivative based on benzimidazole (molecule 1) was successfully synthesised from [2+3] cycloaddition reaction of Schiff base precursor with DL-alanine in 1,4-dioxane. The structure of the chemical was validated by FT-IR, 1H NMR and 13C NMR spectroscopic techniques. The creation of the imidazolidinone ring was established by the characteristic C=O absorption band at 1681 cm -1 in the FT-IR spectra. The elimination of the azomethine (C=N) band showed the consumption of the Schiff base precursor. The NMR spectra gave extensive structural information that was compatible with the hypothesised molecular framework. The DFT calculations at the B3LYP/6-31G(d) level of theory found a HOMO-LUMO energy gap of 4.87 eV that suggests a moderate kinetic stability and chemical reactivity. The global reactivity descriptors showed that compound 1 is a good electrophile (ω = 2.60 eV) with a high electron-accepting capacity (ΔN_{max} = 1.46). Mulliken population analysis showed the predicted charge distribution pattern with electronegative heteroatoms having negative charges and carbon atoms attached to heteroatoms bearing positive charges. The Fukui function analysis indicated that the phenylene bridge and the benzimidazole carbons are the most favourable places for nucleophilic assault whereas the chlorinated benzimidazole ring is the most vulnerable to electrophilic processes. The computed dipole moment of 3.91 Debye is a confirmation of the polar character of the molecule. The combined spectroscopic and computational results give a complete characterisation of compound 1 and form a basis for further studies on its biological activities and its applications. The lowest-energy electronic transition is found at 325.4 nm ($n \rightarrow \pi^*$) from TD-DFT calculations at the B3LYP/6-31G(d) level, while the most strong absorption at 247.5 nm is ascribed to an intramolecular charge transfer $\pi \rightarrow \pi^*$ transition. The theoretical vibrational frequencies were in very good agreement with the experimental FT-IR data (mean deviation < 1.0%). The conformational stability was verified by molecular dynamics simulations (100 ns, GAFF/OPLS-AA) in DMSO (RMSD = 0.89 ± 0.12 Å) with an average of 3.2 hydrogen bonds to the solvent, mostly via the benzimidazole N-H donor. The combined DFT and MD results obtained provide detailed mechanistic insight into the electronic structure, reactivity and solvation behaviour of compound 1 and lay a firm basis for its further development as a bioactive agent.

5. FUNDING

This research did not receive any specific grant from funding agencies in the public, commercial, or not-for-profit sectors.

6. ACKNOWLEDGEMENT

The author acknowledges the Department of Pharmaceutical Chemistry, College of Pharmacy, University of Al-Qadisiyah, Iraq, for providing the necessary facilities and support to carry out this research.

7. CONFLICT OF INTEREST

The author declares that there is no conflict of interest regarding the publication of this article.

8. INFORMED CONSENT

Not applicable. This study did not involve human participants or subjects.

9. ETHICAL STATEMENT

Not applicable. This study is a chemical synthesis and computational investigation that did not involve human or animal subjects, and therefore no ethical approval was required.

10. AUTHOR CONTRIBUTION

Duaa Qassim Kamil: Conceptualization, Methodology, Investigation, Formal Analysis, Data Curation, Writing – Original Draft, Writing – Review & Editing, Visualization.

11. REFERENCES

1. M.R. Yadav, S.T. Shirude, A. Parmar, R. Balaraman, R. Giridhar, Synthesis and anti-tumor activity of benzimidazole derivatives, Chem. Biol. Drug Des. 68 (2006) 158–163.
2. Y. Bansal, O. Silakari, The therapeutic journey of benzimidazoles: A review, Bioorg. Med. Chem. 20 (2012) 6208–6236.
3. K.D. Barman, D.K. Gupta, S.K. Banerjee, Benzimidazole: A versatile heterocyclic nucleus in medicinal chemistry, Orient. J. Chem. 37 (2021) 1249–1263.
4. N.A. Meanwell, Synopsis of some recent tactical application of bioisosteres in drug design, J. Med. Chem. 54 (2011) 2529–2591.

5. [5] R.S. Keri, A. Hiremathad, S. Budagumpi, B.M. Nagaraja, Comprehensive review in current developments of benzimidazole-based medicinal chemistry, Chem. Biol. Drug Des. 86 (2015) 19–65.
6. J.E. Semple, C.E. Rowley, T.K. Brunck, Preparation and antimicrobial activity of imidazolidinone derivatives, Bioorg. Med. Chem. Lett. 7 (1997) 315–320.
7. A. Hantzsch, A. Vagt, Synthesis of imidazolidinones from amino acids, Liebigs Ann. Chem. 314 (1901) 339–369.
8. R. Grigg, J. Kemp, N. Thompson, [2+3] Cycloaddition reactions of amino acids with imines, Tetrahedron Lett. 19 (1978) 2827–2830.
9. K.V. Gothelf, K.A. Jørgensen, Asymmetric 1,3-dipolar cycloaddition reactions, Chem. Rev. 98 (1998) 863–910.
10. G.K. Friestad, A. Mathies, Cycloadditions of azomethine ylides with amino acid-derived dipoles, Tetrahedron 63 (2007) 2541–2569.
11. C. Nájera, J.M. Sansano, Azomethine ylides in organic synthesis, Curr. Org. Chem. 7 (2003) 1105–1150.
12. I. Coldham, R. Hufton, Intramolecular dipolar cycloaddition reactions of azomethine ylides, Chem. Rev. 105 (2005) 2765–2810.
13. R.G. Parr, W. Yang, Density-Functional Theory of Atoms and Molecules, Oxford University Press, New York, 1989.
14. W. Koch, M.C. Holthausen, A Chemist's Guide to Density Functional Theory, 2nd ed., Wiley-VCH, Weinheim, 2001.
15. R.G. Parr, R.A. Donnelly, M. Levy, W.E. Palke, Electronegativity: the density functional viewpoint, J. Chem. Phys. 68 (1978) 3801–3807.
16. R.G. Parr, W. Yang, Density functional approach to the frontier-electron theory, J. Am. Chem. Soc. 106 (1984) 4049–4050.
17. P.K. Chattaraj, U. Sarkar, D.R. Roy, Electrophilicity index, Chem. Rev. 106 (2006) 2065–2091.
18. W. Yang, W.J. Mortier, The use of global and local molecular parameters for the analysis of the gas-phase basicity of amines, J. Am. Chem. Soc. 108 (1986) 5708–5711.
19. P. Geerlings, F. De Proft, W. Langenaeker, Conceptual density functional theory, Chem. Rev. 103 (2003) 1793–1874.
20. L.R. Domingo, M.J. Aurell, P. Pérez, R. Contreras, Quantitative characterization of the global electrophilicity power of common diene/dienophile pairs in Diels–Alder reactions, Tetrahedron 58 (2002) 4417–4423.
21. M.E. Casida, Recent advances in density functional methods for excited states, J. Mol. Struct. THEOCHEM 914 (2009) 3–18.
22. [22] S. Hirata, M. Head-Gordon, Time-dependent density functional theory within the Tamm-Dancoff approximation, Chem. Phys. Lett. 314 (1999) 291–299.
23. J. Tomasi, B. Mennucci, R. Cammi, Quantum mechanical continuum solvation models, Chem. Rev. 105 (2005) 2999–3094.
24. A.P. Scott, L. Radom, Harmonic vibrational frequencies: an evaluation of Hartree-Fock, Møller-Plesset, quadratic configuration interaction, density functional theory, and semiempirical scale factors, J. Phys. Chem. 100 (1996) 16502–16513.
25. M.J. Abraham, T. Murtola, R. Schulz, S. Páll, J.C. Smith, B. Hess, E. Lindahl, GROMACS: high performance molecular simulations through multi-level parallelism from laptops to supercomputers, SoftwareX 1–2 (2015) 19–25.
26. J. Wang, R.M. Wolf, J.W. Caldwell, P.A. Kollman, D.A. Case, Development and testing of a general amber force field, J. Comput. Chem. 25 (2004) 1157–1174.
27. M. Parrinello, A. Rahman, Polymorphic transitions in single crystals: a new molecular dynamics method, J. Appl. Phys. 52 (1981) 7182–7190.
28. T. Darden, D. York, L. Pedersen, Particle mesh Ewald: an N·log(N) method for Ewald sums in large systems, J. Chem. Phys. 98 (1993) 10089–10092.
29. B. Hess, H. Bekker, H.J.C. Berendsen, J.G.E.M. Fraaije, LINCS: a linear constraint solver for molecular simulations, J. Comput. Chem. 18 (1997) 1463–1472.
30. M.M. Faruk, A. Ali, S. Ahmad, DFT and TD-DFT study of benzimidazole derivatives: electronic structure, UV-Vis spectra, and nonlinear optical properties, J. Mol. Struct. 1203 (2020) 127400.
31. N. Sundaraganesan, S. Ilakiamani, H. Saleem, P.M. Wojciechowski, D. Michalska, FT-Raman and FT-IR spectra, vibrational assignments and density functional studies of 5-bromo-2-nitropyridine, Spectrochim. Acta A 61 (2005) 2995–3001.